



NSKY-CD: A System for Cloud Detection Based on Night Sky Brightness and Sky Temperature

Luciano Massetti * , Alessandro Materassi and Francesco Sabatini

Institute of Bioeconomy of the National Research Council, 50019 Sesto Fiorentino, Italy; alessandro.materassi@ibe.cnr.it (A.M.); francesco.sabatini@ibe.cnr.it (F.S.)

* Correspondence: luciano.massetti@ibe.cnr.it; Tel.: +39-055-3033711

Abstract: Cloud cover is important meteorological information that still requires expensive equipment to be monitored from the ground, especially at night. The use of artificial lights at night causes light pollution, and clouds amplify this by reflecting light downward. In addition, cloud thermal radiation emissions affect sky temperature. In this study, we describe a system (NSKY-CD) that can be used to detect clouds at night since it integrates a sky quality meter that measures night sky brightness (NSB) and an air temperature and an infrared temperature sensor that measure sky temperature. We defined a cloud detection method based on fixed threshold values determined with two different procedures that we called ‘optimal’ and ‘antimode’. We then quantitatively assessed the performance of these methods in detecting the presence or absence of clouds in the urban area of Florence during two full moon cycles. Accuracy for the ‘optimal’ method varied between 87% and 91%, while for the ‘antimode’ method, it varied between 86% and 89%. Our results suggest that the two parameters are complementary since NSB has a better performance on moonless nights, and the difference between air temperature and sky temperature has a better performance on moonlit nights. Our method can also be used to analyze historical series of NSB to estimate cloud presence backwards, thus providing important information for meteorological, environmental and astronomical studies.

Keywords: light pollution; cloud detection; clouds; sky glow; infrared thermometer; sensors



Citation: Massetti, L.; Materassi, A.; Sabatini, F. NSKY-CD: A System for Cloud Detection Based on Night Sky Brightness and Sky Temperature. *Remote Sens.* **2023**, *15*, 3063. <https://doi.org/10.3390/rs15123063>

Academic Editors: Martin Aubé and Andreas Jechow

Received: 17 April 2023

Revised: 8 June 2023

Accepted: 8 June 2023

Published: 12 June 2023



Copyright: © 2023 by the authors. Licensee MDPI, Basel, Switzerland. This article is an open access article distributed under the terms and conditions of the Creative Commons Attribution (CC BY) license (<https://creativecommons.org/licenses/by/4.0/>).

1. Introduction

Artificial light at night (ALAN) increases night-sky brightness and is the so-called light pollution that negatively affects astronomical observations and living creatures. In recent decades, light pollution has increased worldwide [1,2] and concern about its environmental impacts within society has grown. Indeed, light pollution and its impacts have become an important field for interdisciplinary scientific debate in these last decades, as evidenced by the growing interest of scientists and the impressive number of publications in astronomy [3,4], marine and terrestrial biology [5–16] and human health [17–19]. One of the most challenging issues is measuring the actual level of light pollution in a specific place and its distribution around the globe. Several approaches are available: satellite remote sensing for assessing light pollution at large spatial scales [20–22], DSLR cameras for assessing light pollution variability in a specific location [23–26] and ground measurement with meters (e.g., SQM and TESS-W) used in stationary monitoring networks [27–33] and moving campaigns [20,34,35]. Moreover, there is growing interest in the investigation of the effects of atmospheric conditions and the presence of clouds since they amplify night sky brightness in light polluted skies. Long time data series of night sky brightness (NSB) show that light pollution is affected by the interaction with natural factors such as moon phase and weather conditions [27,32,36–46].

Indeed, the most important factor affecting night sky brightness is the degree of cloudiness that, especially in polluted sites, enhances skyglow [47]. Moreover, clouds

are one of the dominant sources of atmospheric thermal emissions [48]. Therefore, the presence of clouds can be detected by measuring the infrared radiation emitted downwards with infrared thermal cameras [49–51] and with infrared thermometers for measuring sky temperature [52–54], and the long wave downward radiation [55,56]. Although the influence of clouds on night sky brightness and sky temperature is well known, few studies evaluate methods that use this information for cloud detection. Moreover, most of these studies were focused on how cloud characteristics (e.g., presence, cloud type, height) affect values and variability of these variables more than quantitatively assessing their performance in detecting the presence of clouds. This could be an interesting field for future research because atmospheric clouds are crucial in many theoretical and practical fields [22,57,58]. For instance, cloudiness information for weather forecasting application is provided by ceilometers that estimate the height of the cloud base and other cloud characteristics by emitting near-infrared pulses of light and measuring the delay of the reception of backscattered energy by cloud droplets downwards to the surface [59]. More than 2000 ceilometers [60] are operating in different networks around the world [61–64]. However, the data available from such a network are very limited [60]. For this reason, it might be interesting to integrate the information provided by these devices with low-cost devices that could improve the spatial coverage of cloudiness.

Ground stations can provide information at very high spatial and temporal resolution, but they lack spatial coverage. Conversely, satellite products are characterized by higher spatial coverage, but less spatial resolution and temporal coverage than ground stations. However, a deficit of ground data, especially at night, is still high.

The aim of this study is to present a system, named Night SKY Clouds Detector (NSKY-CD), which is composed of a sky quality meter and an air temperature and thermal infrared thermometer to monitor light pollution and sky temperature, and estimate cloud presence. The NSKY-CD is described in detail and can be easily replicated by other scientists. A second aim is to study the relationship between night sky brightness and temperature indices measured by the NSKY-CD in a polluted site in the Florence metropolitan area, Italy. Our final aim is to quantitatively assess the performance of these variables in estimating cloud presence or absence in the studied site during two full moon cycles. Such a system could provide relevant information about cloudiness that is important for astronomical, environmental and meteorological studies, since they can complement information about cloudiness provided by more expensive systems, such as ceilometers, and can be used for the calibration and validation of satellite products.

2. Materials and Methods

2.1. Description of the System

The NSKY-CD is composed of a temperature and relative humidity sensor, a thermal infrared thermometer and a photometer (Figure 1). The air temperature and relative humidity sensor is a Sensirion SHT85 (<https://sensirion.com/products/catalog/SHT85/>, accessed on 30 April 2023) with RH operating range of 0–100% and accuracy $\pm 1.5\%$; T range from $-40\text{ }^{\circ}\text{C}$ to $+125\text{ }^{\circ}\text{C}$ and accuracy $\pm 0.1\text{ }^{\circ}\text{C}$, size $19 \times 5.6 \times 3.5\text{ mm}^3$ (Figure 1e). The thermal infrared thermometer (IR) is an MLX90614xCC (<https://www.melexis.com/-/media/files/documents/datasheets/mlx90614-datasheet-melexis.pdf>, accessed on 10 June 2023). It measures sky temperature (SkyT) within a temperature range between $-40\text{ }^{\circ}\text{C}$ and $+125\text{ }^{\circ}\text{C}$ for sensor temperature with an accuracy of $0.5\text{ }^{\circ}\text{C}$ in a wide temperature range ($0\text{--}50\text{ }^{\circ}\text{C}$) The field of view is 35° and the wavelength pass band of the optical filter is from 5.5 to $14\text{ }\mu\text{m}$ (Figure 1d,f). We used a SQM-LU-DL sky quality meter (SQM) by Unihedron (<http://unihedron.com>, accessed on 10 June 2023) (Figure 1c), which is a panchromatic sensor that measures night sky brightness (NSB) in magnitude per squared arc second (Mpsas). This unit, used in astronomy, provides the measure of the surface brightness of a unit area of the sky in a negative logarithmic scale. In this scale, a variation of 1 unit accounts for 2.5 times variation of brightness and higher values account for a darker sky due to the negative sign in the function (e.g., 20 Mpsas is 2.5 times

darker than 19 Mpsas). Its spectral response ranges from 320 to 720 nm [41]. Its field of view is 20°. It has a resolution of 0.01 Mpsas and an accuracy of ± 0.1 Mpsas.

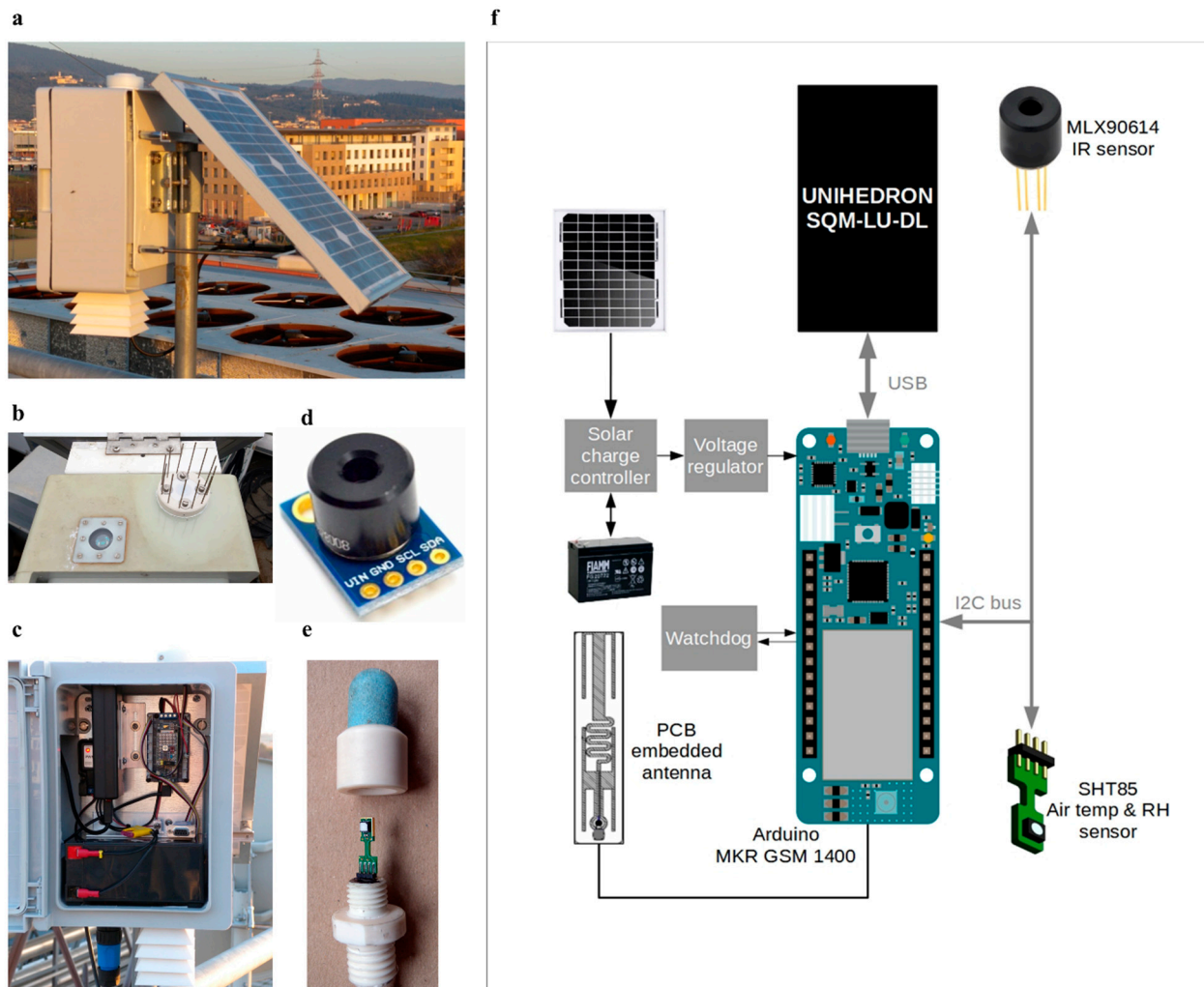


Figure 1. NSKY-CD: view of the whole system with the solar panel (a), view of the top with the openings for the SQM and IR thermometer (b), view of the case with the data logger and sky quality meter (SQM) on the left upper side and the Arduino hardware on the right upper side (c), infrared thermometer (d), sensor of air temperature and relative humidity (e), scheme of the NSKY-CD (f).

The system is controlled by an Arduino MKR GSM 1400 board that acquires data from all the sensors (Figure 1). The system activity can be monitored through a serial port (baud rate 115,200 bit/s).

The NSKY-CD (Figure 1f) is assembled on a case mounted on a pole (Figure 1a). The SQM and IR are pointed upwards to the zenith and are protected by two transparent filters: a polycarbonate screen for the SQM with an attenuation of the signal of 0.1 Mpsas like the screen designed by the manufacturer, and the IR by a white protective window by Edmund Optics designed to be transparent to IR radiation (Figure 1b).

The system can acquire and store data at any time lag. For the purpose of this study, it was set at 5 min, when the value was higher than a threshold of 5 Mpsas. The clock is set to Central European Time (CET). It was synchronized when the system was switched on and, subsequently, once a day with the INRIM ntp server. Once a day the data are transferred to an FTP folder. After successful transfer, the data are deleted from the Arduino memory. The power supply system consists of a 10 W photovoltaic panel, a 12 V 7 Ah lead-acid battery and a charge controller (Figure 1e). The data files, which are in ASCII format with fields separated by commas, are compatible with Campbell Scientific's TOA5 format.

2.2. Data Analysis

An SQM with a polycarbonate screen was compared with an SQM covered by the standard shield provided by the manufacturer. The two systems operated for a month in parallel and the average NSB difference was 0.02 ± 0.11 Mpsas. The NSKY-CD started operating in 2021 on the roof top of CNR Campus (43.817811°N , 11.200117°E), which is located in a heavily polluted night sky area in the middle of the metropolitan area of Florence (Figure 2).

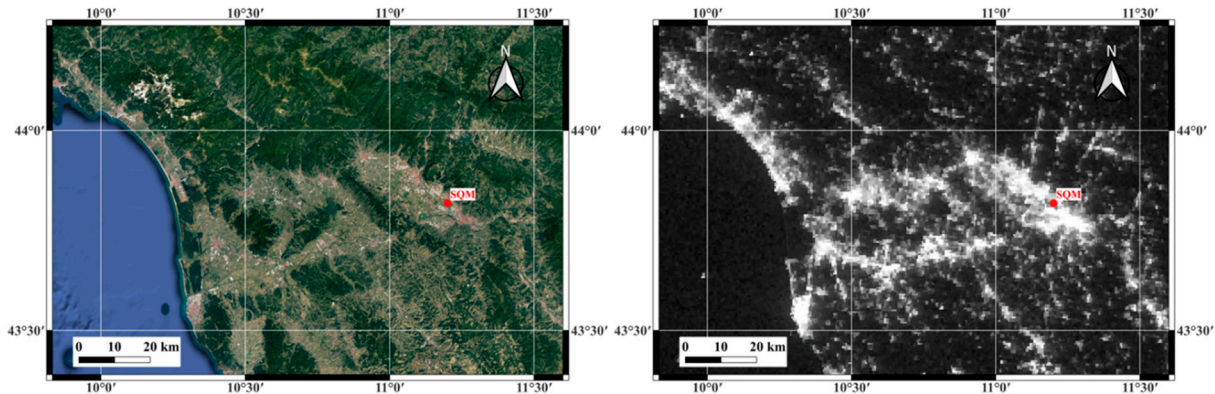


Figure 2. Location of the NSKY-CD sensor (SQM) on Google map and DNB image.

For this study, we used data collected by this system from 5th March to 30th April 2021 (from 00:00 to 04:00 a.m. CET). Records were classified according to moon altitude and moon fraction [32]. Moon fraction (Mfr) is the proportion of moon illuminated by the sun that is visible from a certain location on Earth. Mfr varies from 0 (moonless or moon below the horizon) to 1 (full moon). For this study we classified the dataset on moonless nights (M0) with $Mfr \leq 0.1$ and moonlit nights (M1) with $Mfr > 0.1$. We then used the satellite product Cloud Mask MSG-0 degree (<https://view.eumetsat.int/productviewer?v=default>, accessed on 20 May 2023) to record the presence or absence of clouds over the study area. This product provides images of cloud cover every 15 min with a spatial resolution of $0.041^\circ \times 0.041^\circ$ that approximately corresponds to $4 \text{ km} \times 4 \text{ km}$ in the studied area. Each pixel of the image has a value 0 for clear sky or 1 for cloudy sky. Cloudy sky pixels are also white colored, thus making the identification of cloudy pixels easy and reliable. Therefore, the classification was made by the authors looking at the color of the pixel including the study site (Figure 3) of each image and set the value to C0 if the pixel was not colored and to C1 if the pixel was white.

Each image in the study period was classified according to this criterion, creating a dataset that was used as truth data for cloudy conditions. The final dataset was composed of a total of 917 records, 499 in M0 and 418 in M1, 582 in C0 and 335 in C1 (Table 1).

It is well known that NSB is influenced by the presence of clouds. In light-polluted skies, clouds are illuminated at night by artificial light coming from the ground and therefore, sky brightness increases. This effect is strongly pronounced during moonless nights, while during a full moon, the increase is lower since the sky is already illuminated by the moon. On the contrary, in pristine or scarcely contaminated skies, the effect of clouds is reversed since they block starlight, thus darkening the sky on both moonless and full moon nights. Thermal properties of the sky are also altered by the presence of clouds and their characteristics, such as cloud type and altitude [52]. In this case, the presence of clouds increases the temperature of the sky. For this reason, in this study, night sky brightness (NSB), sky temperature (SkyT) and the difference between sky temperature and air temperature (DeltaT) have been used to estimate presence and absence of clouds. To achieve this goal, we automatically classified sky conditions every 15 min using each of the three variables (NSB, SkyT and DeltaT) to determine one of the two states. The estimated classifications were compared to the classification obtained by MSG-0 images considered as the 'truth'. Sky condition was classified by comparing each 15 min value

with the respective threshold value. Since NSB is strongly amplified by the presence of clouds in highly polluted sites, low Mpsas values are likely associated with the presence of clouds. According to this, sky at time t was classified as C1 if NSB was lower than the NSB threshold and as C0 otherwise. Conversely, sky temperature is higher in the presence of clouds. Therefore, sky at time t was classified as C1 if measured SkyT and DeltaT were higher than their respective thresholds. The capacity to correctly classify the sky condition of each predictor was measured by accuracy (ACC). Accuracy measures the capability of the system to detect both clear and cloudy sky conditions. This index was calculated on a confusion matrix where C0 were considered true negative cases (N) and C1 true positive cases (P). Predicted true positive (TP), true negative (TN), false positive (FP) and false negative (FN) indices were calculated by comparing predicted values with the 'truth'. ACC was then calculated as follows:

$$ACC = (TP + TN)/(P + N)$$

Threshold values were calculated by two different methods. In the first ('optimal'), we applied an iterative process to determine the value of the threshold for each variable that maximizes the accuracy in the studied period.

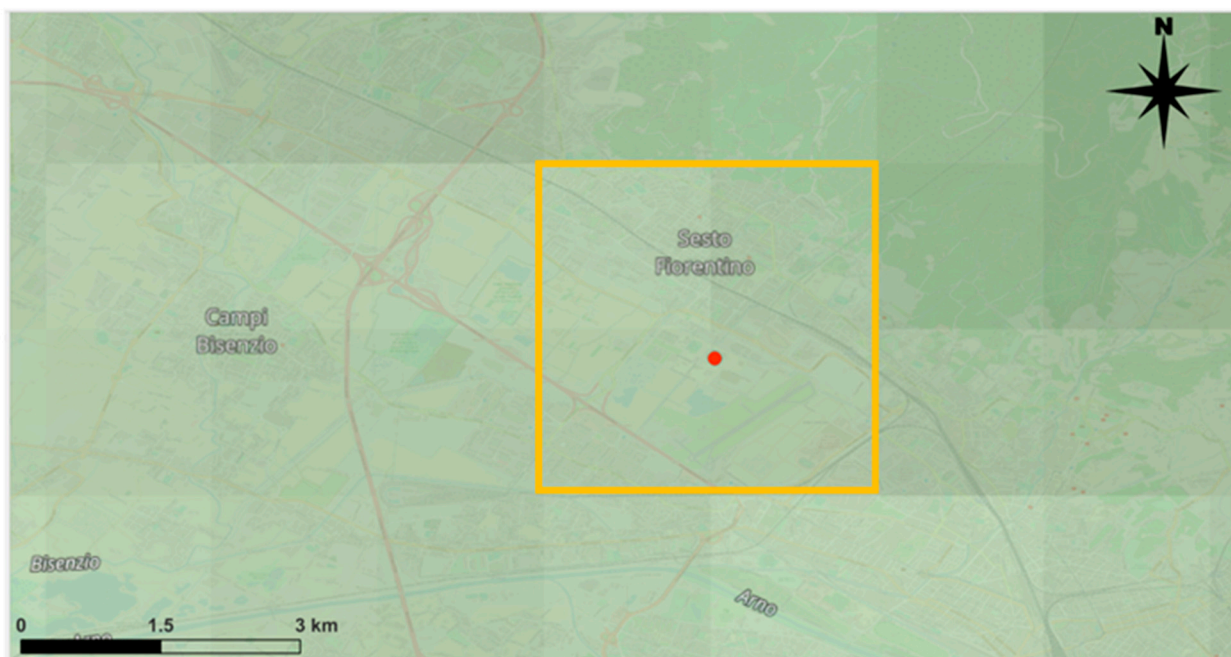


Figure 3. Location of the NSBC-DET sensor (red dot) and the surrounding 4×4 km pixel of Cloud Mask MSG-0 (yellow box).

Table 1. Number of cases for moonless (M0) and moonlit (M1) nights in absence (C0) and presence of clouds (C1).

	M0	M1	Total \times Sky Condition
C0 (absence of clouds)	296	286	582
C1 (presence of clouds)	203	132	335
Total \times moon phase	499	418	917

The optimal thresholds were calculated for the whole dataset (ALL) and the moonless and moonlit sets (M0, M1) (e.g., Figure 4a). However, the 'optimal' method requires a training step to be performed on a reference dataset before its application. For this reason, we proposed and tested a second method to estimate threshold that does not need any training phase, since it is based only on the estimated statistical properties of the dataset

(‘antimode’). This method is based on the assumption that NSB, SkyT and DeltaT follow a bimodal distribution with two peaks corresponding to cloud presence and absence, as the density graphs suggest (e.g., Figure 4b).

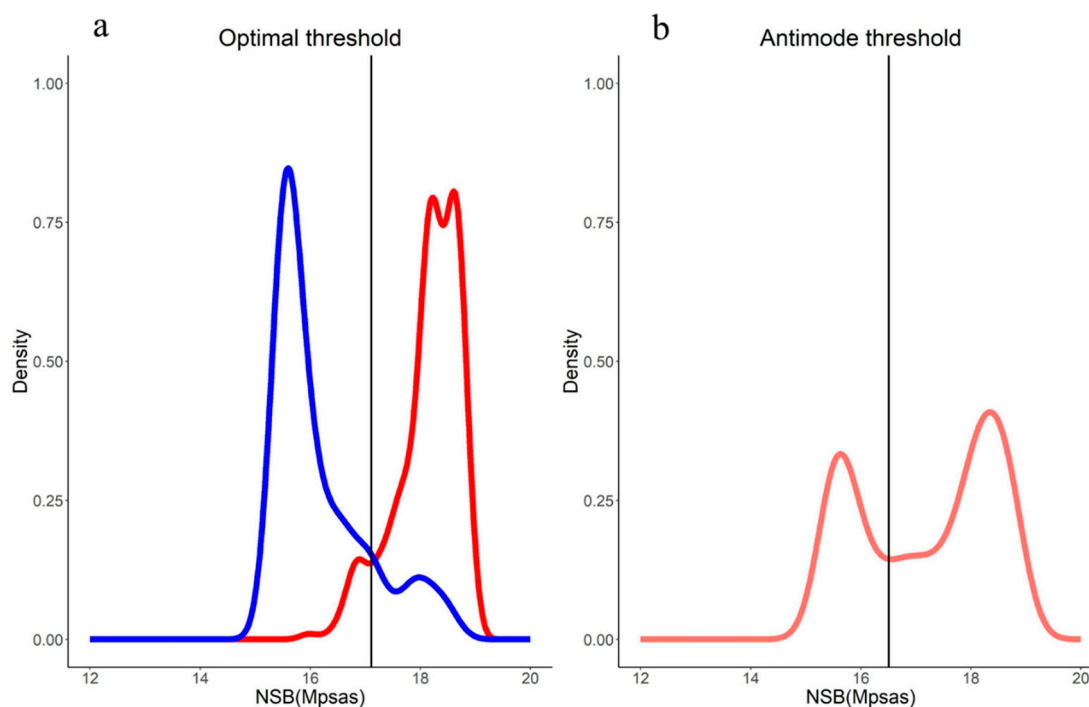


Figure 4. (a) Night sky brightness (NSB) during clear sky (red line) and cloudy sky (blue line) (b) according to our classification method of the MSG-0 product during the study period and the ‘optimal’ NSB threshold (black vertical line) that maximizes the accuracy in cloud detection; (b) Night sky brightness (NSB) during the whole study period (red line) and ‘antimode’ value (black vertical line) of the bimodal distribution that matches the data.

A bimodal distribution is a distribution with two modes that appear as distinct peaks in the distribution, and it has a minimum between them that is called the ‘antimode’. We assumed that all the considered variables (NSB, SkyT and DeltaT) in ALL, M0 and M1 were distributed according to a bimodal distribution of two Gaussian distributions (C0 and C1 subset) and that the ‘antimode’ value of each distribution is the threshold for cloud presence/absence detection (e.g., Figure 4b). Therefore, we calculated the ‘antimode’ value of each distribution and used these values to classify datasets for cloudiness and afterwards to calculate the respective accuracy scores. Linear regression analysis among the monitored variables was also performed.

3. Results

All the density plot of NSB, SkyT and DeltaT present two peaks that can be associated with average values of clear sky (C0) and cloudy sky (C1) conditions (Figure 5). For instance, clear sky is 1.99 Mpsas brighter than cloudy sky on moonless nights and 1.75 Mpsas on moonlit nights (Table 2). Such large NSB differences in clear and cloudy sky conditions confirm that thresholds can be used to detect cloudiness.

Additionally, average SkyT and DeltaT are significantly different between C0 and C1 in both moonless nights and moonlit nights (Table 2). For instance, on clear nights (C0), average SkyT in M1 is approximately 6 °C higher than in M0 and DeltaT in M1 was 2.3 °C higher than in M0 (Table 2). However, these differences might be amplified by the size of our data series. Therefore, a future study on a larger set is needed to assess if the significant difference between moon phases is confirmed or not.

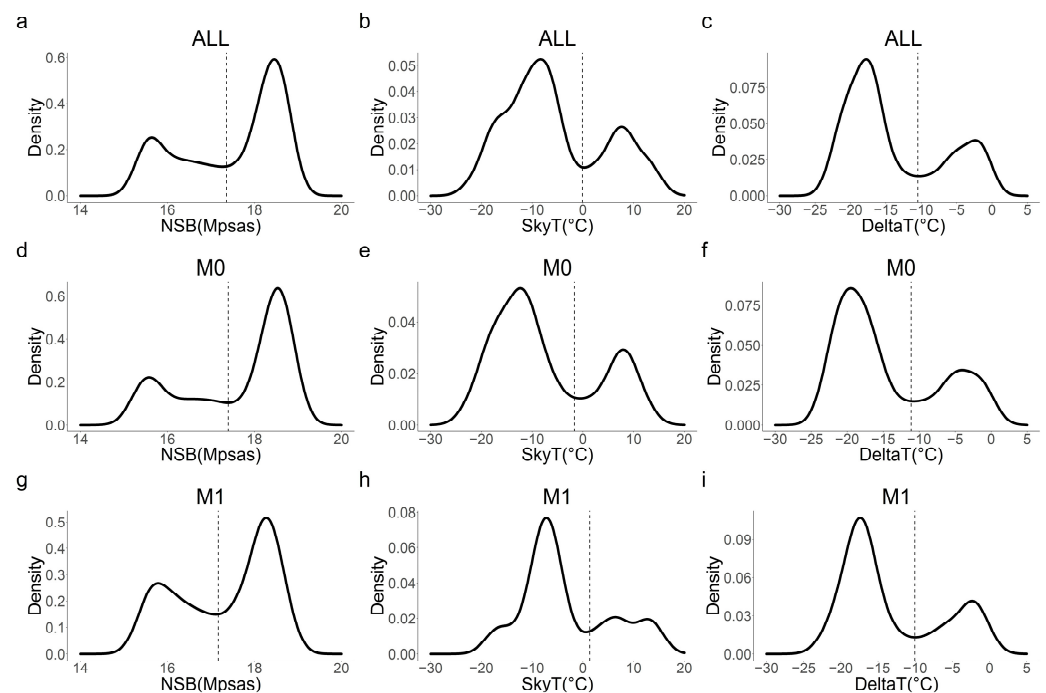


Figure 5. Density plot and ‘antimode’ threshold (vertical line) of night sky brightness (NSB) in Mpsas, sky temperature (SkyT) in °C and sky and ground temperature difference (DeltaT) in °C in the whole (ALL) set (a–c), moonless (M0) set (d–f) and moonlit (M1) set (g–i).

Table 2. Average (Avg) and standard deviation (Sd) of night sky brightness (NSB), sky temperature (SkyT) and sky and ground temperature difference (DeltaT) during moonless clear (M0C0) and cloudy sky (M0C1) and moonlit clear (M1C0) and cloudy sky (M1C1). Significant differences between clear and cloudy sky conditions are reported both for moonless (M0) and moonlit (M1) nights (** $p < 0.01$).

	M0C0 (Avg ± Sd)	M0C1 (Avg ± Sd)	M1C0 (Avg ± Sd)	M1C1 (Avg ± Sd)
NSB (Mpsas)	18.43 ± 0.45 **	16.44 ± 1.01	17.88 ± 0.79 **	16.13 ± 0.61
SkyT (°C)	−13.75 ± 4.79 **	1.90 ± 8.36	−7.68 ± 5.42 **	5.82 ± 7.18
DeltaT (°C)	−18.88 ± 3.01 **	−7.67 ± 6.06	−16.55 ± 4.32 **	−6.14 ± 5.00

NSB and temperature variables are well correlated, and the linear models scored an adjusted R2 varying between 0.86 and 0.91 for the whole dataset (Figure 6a,d,g). Linear relationships between NSB, SkyT and DeltaT were always higher in M0 than in M1 set (Figure 6).

Cloud Detection Accuracy

Cloud detection accuracy, obtained for the whole set (ALL) by using the ‘optimal’ threshold of each variable, varied from 0.87 (NSB) to 0.89 (DeltaT) (Figure 7, Table 3). When moon phases were considered separately, ‘optimal’ thresholds scored higher accuracies: from 0.89 (SkyT) to 0.91 (NSB) on moonless nights and from 0.89 to 0.90 on moonlit nights (Table 3). ‘Optimal’ threshold values varied according to moon presence (Table 3, Figure 4). For this reason, the accuracy is improved if moonless and moonlit sets are considered separately, especially for NSB that is very sensitive to moon presence [36]. Indeed, the brightness of the moon is comparable to the brightness due to the clouds, thus making it more difficult to assess the cause of high brightness values if moon phases are not considered separately (Table 3). On the contrary, DeltaT ‘optimal’ thresholds and accuracy is less affected by considering M0 and M1 sets separately or not (Table 3). Summing up, NSB is the most effective parameter for cloud detection for M0, while DeltaT is the most effective both for ALL and M1 sets.

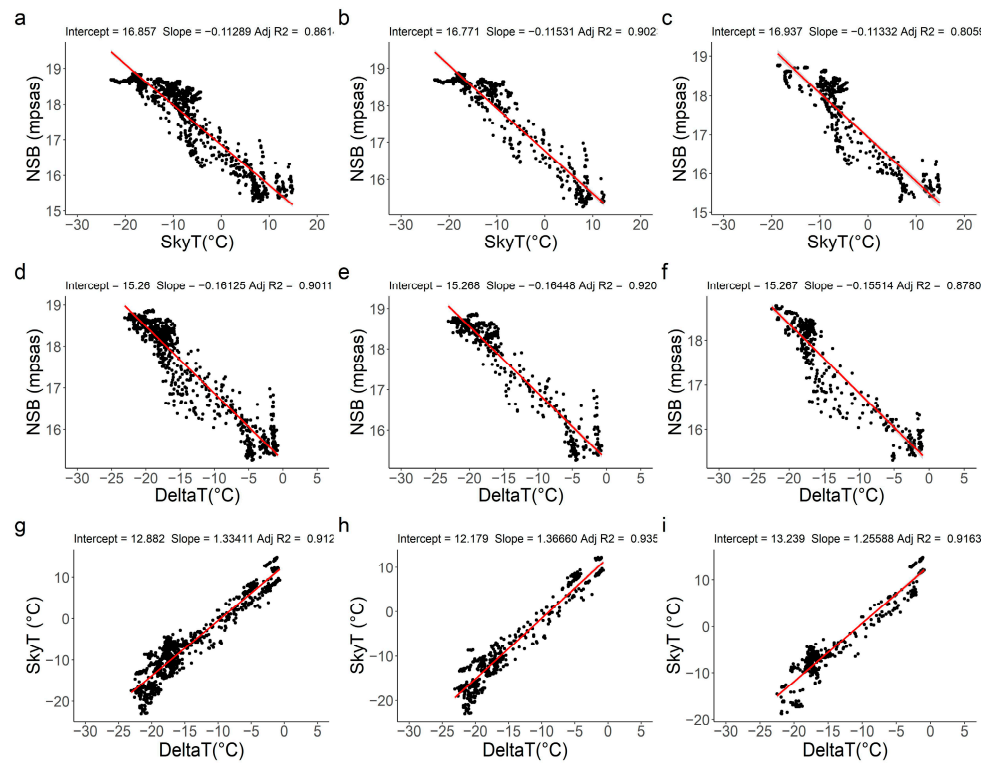


Figure 6. Relationship between night sky brightness (NSB), sky temperature (SkyT) and difference between sky temperature and air temperature (DeltaT) for the whole (ALL) set (a,d,g), for moonless (MO) set (b,e,h) and moonlit (M1) set (c,f,i). The red lines represent the linear regression lines. Intercept, slope and adjusted R2 coefficients of the linear models are reported on top of each graph.

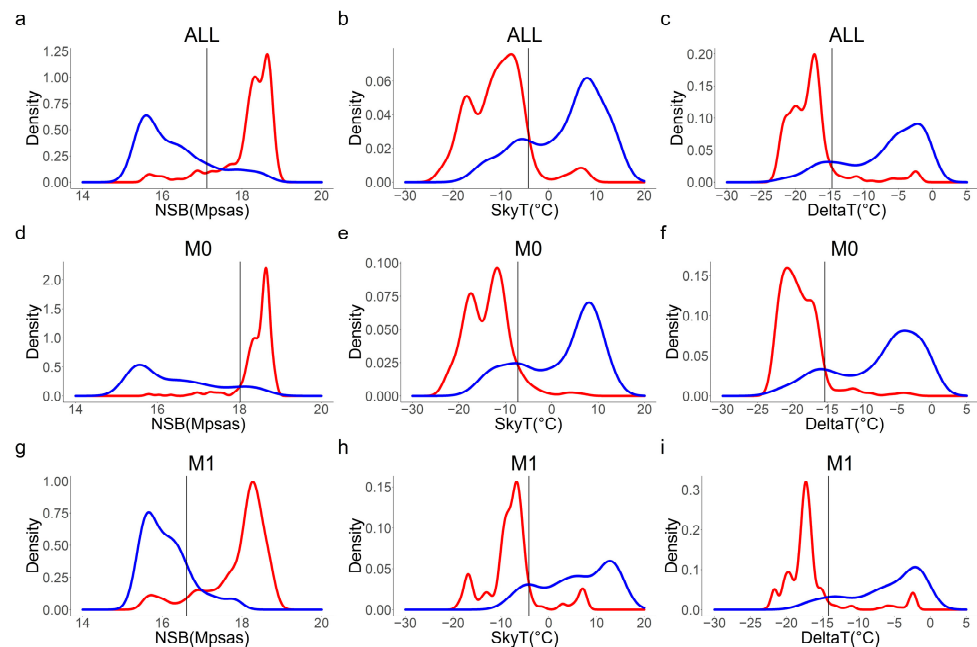


Figure 7. Density plot and 'optimal' threshold value (vertical line) of night sky brightness (NSB) in Mpsas, sky temperature (SkyT) in °C and sky and ground temperature difference (DeltaT) in °C for clear sky (C0, blue line) and cloudy sky (C1 red line), the whole (ALL) set (a–c) and moonless (M0) set (d–f) and moonlit (M1) set (g–i).

Table 3. Accuracy (ACC) in predicting presence/absence of clouds in the study period for the whole (ALL), moonless (M0) and moonlit (M1) sets using ‘optimal’ and ‘antimode’ thresholds of night sky brightness (NSB), sky temperature (SkyT) and difference between sky temperature and air temperature (DeltaT).

Set	Parameter	Optimal Threshold	ACC	Antimode Threshold	ACC
ALL	NSB (MPSAS)	17.12	0.87	17.36	0.87
	SkyT (°C)	−4.24	0.88	−0.09	0.86
	DeltaT (°C)	−14.67	0.89	−10.48	0.87
M0	NSB (MPSAS)	18.02	0.91	17.4	0.89
	SkyT (°C)	−7.27	0.88	−1.67	0.86
	DeltaT (°C)	−15.34	0.89	−11.11	0.87
M1	NSB (MPSAS)	16.61	0.89	17.17	0.86
	SkyT (°C)	−4.12	0.89	1.36	0.86
	DeltaT (°C)	−14.16	0.90	−10.05	0.87

Cloud detection accuracy using ‘antimode’ values (Figure 5) is still high, even though slightly lower than the ‘optimal’. NSB performed slightly better than the others on moonless nights, while DeltaT performed slightly better when moon phase was not considered.

Therefore, the variability of NSB and DeltaT can be used as proxy for cloud presence/absence in light polluted sites.

4. Discussion

Several studies assessed that cloudiness affects night sky brightness values in both light polluted and pristine sites. However, to our knowledge, the effective performance of NSB in estimating night cloudiness has been poorly tested. The NSKY-CD is composed of a sky quality meter and an IR sensor that can also be used to detect the presence of clouds. We tested it in a polluted site, where the NSB difference between clear and cloudy sky were comparable with other studies. We found 1.99 Mpsas and 1.75 Mpsas difference, respectively, on moonless and moonlit nights. For instance, average differences of 1.92 Mpsas were found in Barcelona [27] and 2.8 Mpsas difference in Potsdam-Babelsberg [36]. Some studies assessed that NSB difference depends on cloud height and can decrease to 0.9 Mpsas for high clouds [27,47], suggesting that in these cases discriminating between clear and cloudy sky only on the basis of a fixed threshold could be very difficult.

We found an average difference of DeltaT between clear and cloudy sky of about 11°C for M0 and 10 °C for M1. One study [54] found higher differences of 11 °C and 18 °C according to cloud type but measures were collected both during day and nighttime. Another study [53] also found larger short-scale variation and higher IR sky temperature in cloudy conditions.

Our system uses three variables (NSB, SkyT and DeltaT) that are effective in detecting the presence/absence of clouds. We applied two methods based on fixed thresholds (‘optimal’ and ‘antimode’) on the whole dataset and on moonless and moonlit sets separately. Accuracy was always higher than 0.86, which means that more than 86% of the records were correctly classified for presence/absence of clouds in the worst case and this performance is improved to 91% and 90%, respectively, if moonless and moonlit data are analyzed separately. The implementation of the ‘antimode’ method is less complex than the ‘optimal’ method since it does not require any training phase and the threshold can be derived directly from the data distribution. The performance is slightly worse than for the ‘optimal’ method (Table 3) because the assumption of bimodal distribution is poorly met in some cases, such as for SkyT in M1 (Figure 5). Our results suggest that NSB performs better on moonless nights and DeltaT on moonlit nights (Table 3).

However, we expected a greater difference in the performance of M0 compared to M1 that is affected by the mixing of the amplifying effect of the moon and clouds. For this reason, we focused our attention on wrong classifications (FP and FN). In M0, we found a relevant number of cases that were erroneously classified as clear using NSB (11 out of 41). For those cases the measured values ranged from 18.41 to 18.72 Mpsas that were distributed in the upper part of the moonless and clear sky distribution (Table 2, Figure 5), while in the satellite images those records were marked as cloudy. The same problem was found for the classification made with DeltaT. Again, measured values of 11 out of 41 FN cases ranged from $-18.7\text{ }^{\circ}\text{C}$ to $-22.2\text{ }^{\circ}\text{C}$ and were distributed in the lower part of DeltaT distribution (Table 2, Figure 5). Since, in most of these cases, the three methods provide the same classification that is different from the reference set, the question arises whether ground-based systems detect clouds better than satellite-based systems. For this reason, we used the Kendall's coefficient of concordance test (W) [65] to measure the level of agreement among the three parameters (NSB, SkyT and DeltaT) with the optimal threshold method and the reference set. Kendall's coefficient of concordance ranges from 0 (no agreement) to 1 (complete agreement). Comparing all the methods and the reference set we obtained $W = 0.867$. If in turn, we compare three of the four classifications we obtain the highest concordance among the three parameters $W = 0.920$, while between two parameters and the reference set it varies between $W = 0.861$ and $W = 0.865$. The higher concordance level between methods based on three different variables suggests that further investigations are needed using a more reliable dataset as reference, for example direct observation of the sky or other information derived from satellite images or ceilometers.

However, erroneous classifications are likely associated with the fact that clouds of different types and heights cause different amplification of ALAN and different sky temperatures. Indeed, some studies assessed that both sky temperature and zenith night sky brightness are only slightly affected by the presence of cirrus clouds [53,58] since they are colder than low clouds and optically thinner, thus reflecting less light. Furthermore, a previous study conducted at a site near Krakow (Poland) assessed that average NSB varied from 17.9 Mpsas (e.g., nimbostratus) to 19.5 Mpsas (e.g., cirrostratus) according to the type and height of the clouds [44]. Such a broad range of variation of the amplifying effect due to clouds indicates that their presence cannot be detected by using a fixed threshold value. Therefore, cloud type and height should be considered when determining the thresholds to improve the performance of these methods. For this scope, other satellite products should also be considered in the future since cloud mask products do not provide such detailed information.

The system and detecting methods have been tested only in one polluted site, where the brightening effect of clouds is strong and allows sky conditions to be easily discriminated. The fixed thresholds are site dependent, but the methods to calculate them can be easily applied to any polluted night sky site. Future studies are needed to investigate if this method can be extended to sites with a lower level of light pollution and to pristine ones where cloudiness reduces night sky brightness and the variation in intensity is lower than in polluted sites and can take into account the seasonal variation of temperature, moon phases and increasing trends of light pollution through the analysis of long-time data series.

Another thread of investigation could be the use of indices of short-term variability of night sky brightness or sky temperature (e.g., standard deviation of the variable) for cloud detection, as has been proposed by other studies [42,53]. However, this method requires high frequency measurements that are not often available, especially for historical and current data series. In the future, it would be worth testing the performance of detection methods based on the combination of threshold values and short-term variability of NSB and DeltaT.

5. Conclusions

The NSKY-CD is a ground system that can cover the lack of information about the presence of clouds at night. This system is low-cost and easy to build and install. It is

designed to operate autonomously in remote places due to its solar energy system supply and data transmission technology. We tested cloud detection methods based on ‘optimal’ and ‘antimode’ threshold values of three variables (NSB, SkyT and DeltaT). We found that these variables can complement each other whilst performing cloud detection since NSB better detects clouds on moonless nights and DeltaT on moonlit nights. The system is very versatile because in addition to being used for monitoring night sky brightness continuously and studying its trend over the year, its seasonal variability and moon cycles, it can also be used for detecting cloudiness at night.

The environmental variables measured by our system in a light-polluted site were clearly affected by the presence of clouds, as shown by the bimodal distribution of the data. All the variables were significantly affected by clouds on moonless and moonlit nights. Therefore, threshold values determined through a training process or by using the statistical property of the bimodal distribution allow the presence or absence of clouds to be detected with a high level of accuracy. This suggests that analysis of the data collected by the proposed system can be used for cloud detection and applied, at least for the NSB data, backwards to a large number of data sets available all over the world.

This type of data is important for astronomical, environmental and meteorological studies, for instance, in ecological studies where the presence of clouds and their amplifying effect of light pollution can damage sensitive species. These low-cost systems can provide information that can complement the information provided by more expensive ground-based systems for cloud detection, such as ceilometers, and could be used to calibrate and validate satellite products.

Author Contributions: Conceptualization, L.M. and A.M.; methodology, L.M.; validation, L.M., A.M. and F.S.; formal analysis, L.M.; investigation, L.M., A.M. and F.S.; data curation, L.M. and A.M.; writing—original draft preparation, L.M., A.M. and F.S.; writing—review and editing, L.M.; supervision, L.M.; project administration, L.M. and F.S. All authors have read and agreed to the published version of the manuscript.

Funding: This research received no external funding.

Data Availability Statement: The data presented in this study are openly available in Zenodo at <https://doi.org/10.5281/zenodo.7982297>.

Acknowledgments: The authors wish to thank Dino Ferrini, teacher of Mathematics at Istituto Tecnico Professionale “Margaritone” of Arezzo, Italy, since his suggestions were helpful in improving this study.

Conflicts of Interest: The authors declare no conflict of interest.

References

1. Kyba, C.C.; Tong, K.P.; Bennie, J.; Birriel, I.; Birriel, J.J.; Cool, A.; Gaston, K.J. Worldwide variations in artificial skyglow. *Sci. Rep.* **2015**, *5*, 8409. [[CrossRef](#)] [[PubMed](#)]
2. Falchi, F.; Cinzano, P.; Duriscoe, D.; Kyba, C.C.M.; Elvidge, C.D.; Baugh, K.; Portnov, B.A.; Rybnikova, N.A.; Furgoni, R. The new world atlas of artificial night sky brightness. *Sci. Adv.* **2016**, *2*, e1600377. [[CrossRef](#)] [[PubMed](#)]
3. Duriscoe, D.; Luginbuhl, C.; Elvidge, C. The relation of outdoor lighting characteristics to sky glow from distant cities. *Light. Res. Technol.* **2014**, *46*, 35–49. [[CrossRef](#)]
4. Falchi, F.; Bara, S. A linear systems approach to protect the night sky: Implications for current and future regulations. *R. Soc. Open Sci.* **2020**, *7*, 6–9. [[CrossRef](#)]
5. Gaston, K.J.; Duffy, J.P.; Bennie, J. Quantifying the erosion of natural darkness in the global protected area system: Decline of darkness within protected areas. *Conserv. Biol.* **2015**, *29*, 1132–1141. [[CrossRef](#)]
6. Ffrench-Constant, R.H.; Somers-Yeates, R.; Bennie, J.; Economou, T.; Hodgson, D.; Spalding, A.; McGregor, P.K. Light pollution is associated with earlier tree budburst across the United Kingdom. *Proc. R. Soc. B Biol. Sci.* **2016**, *283*, 20160813. [[CrossRef](#)] [[PubMed](#)]
7. Bennie, J.; Davies, T.W.; Cruse, D.; Gaston, K.J. Ecological effects of artificial light at night on wild plants. *J. Ecol.* **2016**, *104*, 611–620. [[CrossRef](#)]

8. Škvareninová, J.; Tuhárska, M.; Škvarenina, J.; Babálová, D.; Slobodníková, L.; Slobodník, B.; Středová, H.; Mindaš, J. Effects of light pollution on tree phenology in the urban environment. *Morav. Geogr. Rep.* **2017**, *25*, 282–290. [[CrossRef](#)]
9. Bennie, J.; Davies, T.W.; Cruse, D.; Inger, R.; Gaston, K.J. Artificial light at night causes top-down and bottom-up trophic effects on invertebrate populations. *J. Appl. Ecol.* **2018**, *55*, 2698–2706. [[CrossRef](#)]
10. Dimitriadis, C.; Fournari-Konstantinidou, I.; Sourbèsa, L.; Koutsoubas, D.; Mazaris, A.D. Reduction of sea turtle population recruitment caused by nightlight: Evidence from the Mediterranean region. *Ocean Coast. Manag.* **2018**, *153*, 108–115. [[CrossRef](#)]
11. Massetti, L. Assessing the impact of street lighting on *Platanus x acerifolia* phenology. *Urban For. Urban Green.* **2018**, *34*, 71–77. [[CrossRef](#)]
12. Grubisic, M.; Haim, A.; Bhusal, P.; Dominoni, D.M.; Gabriel, K.M.A.; Jechow, A.; Kupprat, F.; Lerner, A.; Marchant, P.; Riley, W.; et al. Light pollution, circadian photoreception, and melatonin in vertebrates. *Sustainability* **2019**, *11*, 6400. [[CrossRef](#)]
13. Grubisic, M.; van Grunsven, R.H.A.; Kyba, C.C.M.; Manfrin, A.; Hölker, F. Insect declines and agroecosystems: Does light pollution matter? Insect declines and agroecosystems. *Ann. Appl. Biol.* **2018**, *173*, 180–189. [[CrossRef](#)]
14. Maggi, E.; Bongiorno, L.; Fontanini, D.; Capocchi, A.; Dal Bello, M.; Giacomelli, A.; Benedetti Cecchi, L. Artificial light at night erases positive interactions across trophic levels. *Funct. Ecol.* **2020**, *34*, 694–706. [[CrossRef](#)]
15. Dominoni, D.M.; Smit, J.A.H.; Visser, M.E.; Halfwerk, W. Multisensory pollution: Artificial light at night and anthropogenic noise have interactive effects on activity patterns of great tits (*Parus major*). *Environ. Pollut.* **2020**, *256*, 113314. [[CrossRef](#)]
16. Yang, Y.; Liu, Q.; Wang, T.; Pan, J. Light pollution disrupts molecular clock in avian species: A power-calibrated meta-analysis. *Environ. Pollut.* **2020**, *265*, 114206. [[CrossRef](#)]
17. Haim, A.; Zubidat Abed, E. Artificial light at night: Melatonin as a mediator between the environment and epigenome. *Philos. Trans. R. Soc. B Biol. Sci.* **2015**, *370*, 20140121. [[CrossRef](#)]
18. Touitou, Y.; Reinberg, A.; Touitou, D. Association between light at night, melatonin secretion, sleep deprivation, and the internal clock: Health impacts and mechanisms of circadian disruption. *Life Sci.* **2017**, *173*, 94–106. [[CrossRef](#)]
19. Svechkina, A.; Portnov, B.A.; Trop, T. The impact of artificial light at night on human and ecosystem health: A systematic literature review. *Landsc. Ecol.* **2020**, *35*, 1725–1742. [[CrossRef](#)]
20. Katz, Y.; Levin, N. Quantifying urban light pollution-A comparison between field measurements and EROS-B imagery. *Remote Sens. Environ.* **2016**, *177*, 65–77. [[CrossRef](#)]
21. Levin, N.; Kyba, C.C.M.; Zhang, Q.; Sánchez de Miguel, A.; Román, M.O.; Li, X.; Portnov, B.A.; Molthan, A.L.; Jechow, A.; Miller, S.D.; et al. Remote sensing of night lights: A review and an outlook for the future. *Remote Sens. Environ.* **2020**, *237*, 111443. [[CrossRef](#)]
22. Barentine, J.C.; Walczak, K.; Gyuk, G.; Tarr, C.; Longcore, T. A case for a new satellite mission for remote sensing of night lights. *Remote Sens.* **2021**, *13*, 2294. [[CrossRef](#)]
23. Solano Lampar, H.A.; Kocifaj, M. Urban artificial light emission function determined experimentally using night sky images. *J. Quant. Spectro. Radiat. Trans.* **2016**, *181*, 87–95. [[CrossRef](#)]
24. Kolláth, Z.; Dömény, A. Night sky quality monitoring in existing and planned dark sky parks by digital cameras. *Int. J. Sustain. Light* **2017**, *19*, 61–68. [[CrossRef](#)]
25. Jechow, A.; Ribas, S.J.; Domingo, R.C.; Hölker, F.; Kolláth, Z.; Kyba, C.C.M. Tracking the dynamics of skyglow with differential photometry using a digital camera with fisheye lens. *J. Quant. Spectrosc. Radiat. Transf.* **2018**, *209*, 212–223. [[CrossRef](#)]
26. Jechow, A.; Hölker, F.; Kyba, C.C.M. Using all-sky differential photometry to investigate how nocturnal clouds darken the night sky in rural areas. *Sci. Rep.* **2019**, *9*, 1391. [[CrossRef](#)]
27. Ribas, S.J.; Figueras, F.; Pascio, S.; Canal-Domingo, R.; Torra, J. How clouds are amplifying (or not) the effects of ALAN. *Int. J. Sustain. Light.* **2016**, *35*, 32–39. [[CrossRef](#)]
28. Posch, T.; Binder, F.; Puschnig, J. Systematic measurements of the night sky brightness at 26 locations in Eastern Austria. *J. Quant. Spectro. Radiat. Trans.* **2018**, *211*, 144–165. [[CrossRef](#)]
29. Bará, S.; Lima, R.C.; Zamorano, J. Monitoring long-term trends in the anthropogenic night sky brightness. *Sustainability* **2019**, *11*, 3070. [[CrossRef](#)]
30. Bertolo, A.; Binotto, R.; Ortolani, S.; Sapienza, S. Measurements of night sky brightness in the Veneto Region of Italy: Sky quality meter network results and differential photometry by digital single lens reflex. *J. Imaging* **2019**, *5*, 56. [[CrossRef](#)]
31. Zamorano, J.; Tapia, C.; Pascual, S.; García, C.; González, R.; González, E.; Corcho, O.; García, L.; Gallego, J.; Sánchez de Miguel, A.; et al. Night Sky Brightness Monitoring in Spain. In *Highlights on Spanish Astrophysics X, Proceedings of the XIII Scientific Meeting of the Spanish Astronomical Society, Salamanca, Spain, 16–20 July 2018*; Montesinos, B., Asensio Ramos, A., Buitrago, F., Schödel, R., Villaver, E., Pérez-Hoyos, S., Ordóñez-Etxeberria, I., Eds.; Sociedad Española de Astronomía: Salamanca, Spain, 2019; pp. 599–604. ISBN 978-84-09-09331-1.
32. Massetti, L. Drivers of artificial light at night variability in urban, rural and remote areas. *J. Quant. Spectro. Radiat. Trans.* **2020**, *255*, 107250. [[CrossRef](#)]
33. Karpińska, D.; Kunz, M. Device for automatic measurement of light pollution of the night sky. *Sci. Rep.* **2022**, *12*, 16476. [[CrossRef](#)] [[PubMed](#)]
34. Caruana, J.; Vella, R.; Spiteri, D.; Nolle, M.; Fenech, S.; Aquilina, N.J. A photometric mapping of the night sky brightness of the Maltese islands. *J. Environ. Manag.* **2020**, *261*, 110196. [[CrossRef](#)] [[PubMed](#)]

35. Karpińska, D.; Kunz, M. Vertical variability of night sky brightness in urbanised areas. *Quaest. Geogr.* **2023**, *42*, 5–14.
36. Kyba, C.C.M.; Ruhtz, T.; Fischer, J.; Hölker, F. Cloud coverage acts as an amplifier for ecological light pollution in urban ecosystems. *PLoS ONE* **2011**, *6*, e17307. [[CrossRef](#)] [[PubMed](#)]
37. Kocifaj, M.; Solano Lamphar, H.A. Quantitative analysis of night skyglow amplification under cloudy conditions. *Mon. Not. R. Astron. Soc.* **2014**, *443*, 3665–3674. [[CrossRef](#)]
38. Aubé, M.; Kocifaj, M.; Zamorano, J.; Lamphar, H.S.; de Miguel, A.S. The spectral amplification effect of clouds to the night sky radiance in Madrid. *J. Quant. Spectro. Radiat. Trans.* **2016**, *181*, 11–23. [[CrossRef](#)]
39. Jechow, A.; Kolláth, Z.; Ribas, S.J.; Spoelstra, H.; Hölker, F.; Kyba, C.C.M. Imaging and mapping the impact of clouds on skyglow with all-sky photometry. *Sci. Rep.* **2017**, *7*, 6741. [[CrossRef](#)]
40. Kyba, C.C.M.; Mohar, A.; Posch, T. How bright is moonlight? *Astron. Geophys.* **2017**, *58*, 31–32. [[CrossRef](#)]
41. Kotarba, Z.A.; Chacewicz, S.; Zmudzka, E. Night sky photometry over Warsaw (Poland) evaluated simultaneously with surface-based and satellite-based cloud observations. *J. Quant. Spectro. Radiat. Trans.* **2019**, *235*, 95–107. [[CrossRef](#)]
42. Cavazzani, S.; Ortolani, S.; Bertolo, A.; Binotto, R.; Fiorentin, P.; Carraro, G.; Saviane, I.; Zitelli, V. Sky Quality Meter and satellite correlation for night cloud-cover analysis at astronomical sites. *Mon. Not. R. Astron. Soc.* **2020**, *493*, 2463–2471. [[CrossRef](#)]
43. Puschnig, J.; Wallner, S.; Posch, T. Circalunar variations of the night sky brightness—An FFT perspective on the impact of light pollution. *Mon. Not. R. Astron. Soc.* **2020**, *492*, 2622–2637. [[CrossRef](#)]
44. Sciezor, T. The impact of clouds on the brightness of the night sky. *J. Quant. Spectrosc. Radiat. Transf.* **2020**, *247*, 106962. [[CrossRef](#)]
45. Marseille, C.; Aubé, M.; Barreto, A.; Simoneau, A. Remote sensing of aerosols at night with the CoSQM sky brightness data. *Remote Sens.* **2021**, *13*, 4623. [[CrossRef](#)]
46. Puschnig, J.; Wallner, S.; Schwöpe, A.; Naslund, M. Long-term trends of light pollution assessed from SQM measurements and an empirical atmospheric model(dagger). *Mon. Not. R. Astron. Soc.* **2023**, *518*, 4449–4465. [[CrossRef](#)]
47. Puschnig, J.; Schwöpe, A.; Posch, T.; Schwarz, R. The night sky brightness at Potsdam-Babelsberg including overcast and moonlit conditions. *J. Quant. Spectrosc. Radiat. Transf.* **2014**, *139*, 76–81. [[CrossRef](#)]
48. Shaw, J.; Nugent, P.; Pust, N.; Thurairajah, B.; Mizutani, K. Radiometric cloud imaging with an uncooled microbolometer thermal infrared camera. *Opt. Express.* **2005**, *13*, 5807–5817. [[CrossRef](#)]
49. Thurairajah, B.; Shaw, J.A. Cloud statistics measured with the infrared cloud imager. *IEEE Trans. Geosci. Remote Sens.* **2005**, *43*, 2000–2007. [[CrossRef](#)]
50. Lagrosas, N.; Shiina, T.; Kuze, H. Observations of nighttime clouds over Chiba, Japan, using digital cameras and satellite images. *J. Geophys. Res. Atmos.* **2021**, *126*, D034772. [[CrossRef](#)]
51. Wang, Y.; Liu, D.; Xie, W.; Yang, M.; Gao, Z.; Ling, X.; Huang, Y.; Li, C.; Liu, Y.; Xia, Y. Day and night clouds detection using a thermal-infrared all-sky-view camera. *Remote Sens.* **2021**, *13*, 1852. [[CrossRef](#)]
52. Riordan, D.; Clay, R.W.; Maghrabi, A.H.; Dawson, B.; Wild, N. Cloud base temperature measurements using a simple longwave infrared cloud detection system. *J. Geophys. Res. Atmos.* **2005**, *110*, D03207. [[CrossRef](#)]
53. Brocard, E.; Schneebeli, M.; Mätzler, C. Detection of cirrus clouds using infrared radiometry. *IEEE Trans. Geosci. Remote Sens.* **2011**, *49*, 595–602. [[CrossRef](#)]
54. Maghrabi, A. Modification of the IR sky temperature under different atmospheric conditions in an arid region in central Saudi Arabia: Experimental and theoretical justification. *J. Geophys. Res. Atmos.* **2012**, *17*, D19. [[CrossRef](#)]
55. Dürr, B.; Philipona, R. Automatic cloud amount detection by surface longwave downward radiation measurements. *J. Geophys. Res.* **2004**, *109*, D05201. [[CrossRef](#)]
56. González, J.-A.; Calbó, J.; Sola, Y. Assessment of cloudless-to-cloud transition zone from downwelling longwave irradiance measurements. *Atmos. Res.* **2023**, *285*, 106657. [[CrossRef](#)]
57. Gaston, K.J. Nighttime ecology: The “Nocturnal Problem” revisited. *Am. Nat.* **2019**, *193*, 481–502. [[CrossRef](#)]
58. Kómar, L.; Necas, A. Effect of cloud micro-physics on zenith brightness in urban environment. *J. Quant. Spectrosc. Radiat. Transf.* **2023**, *302*, 108563. [[CrossRef](#)]
59. Wagner, T.J.; Kleiss, J.M. Error characteristics of ceilometer-based observations of cloud amount. *J. Atmos. Ocean. Technol.* **2016**, *33*, 1557–1567. [[CrossRef](#)]
60. Thomas, W. European ceilometer and lidar networks for aerosol profiling and aviation safety—The German contribution. In Proceedings of the 2017 WMO Aeronautical Meteorology Scientific Conference, Toulouse, France, 6–10 November 2017; Available online: https://library.wmo.int/doc_num.php?explnum_id=4444 (accessed on 26 May 2023).
61. Illingworth, A.J.; Hogan, R.J.; O’connor, E.J.; Bouniol, D.; Brooks, M.E.; Delanoë, J.; Wrench, C.L. Cloudnet: Continuous evaluation of cloud profiles in seven operational models using groundbased observations. *Bull. Am. Meteorol. Soc.* **2007**, *88*, 883–898. [[CrossRef](#)]
62. Martucci, G.; Milroy, C.; O’Dowd, C.D. Detection of cloud-base height using Jenoptik CHM15K and Vaisala CL31 ceilometers. *J. Atmos. Ocean. Technol.* **2010**, *27*, 305–318. [[CrossRef](#)]
63. Dionisi, D.; Barnaba, F.; Diémoz, H.; Di Liberto, L.; Gobbi, G.P. A multiwavelength numerical model in support of quantitative retrievals of aerosol properties from automated lidar ceilometers and test applications for AOT and PM10 estimation. *Atmos. Meas. Tech.* **2018**, *11*, 6013–6042. [[CrossRef](#)]

64. Pîrloagă, R.; Ene, D.; Boldeanu, M.; Antonescu, B.; O'Connor, E.J.; Ștefan, S. Ground-based measurements of cloud properties at the Bucharest–Măgurele Cloudnet Station: First results. *Atmosphere* **2022**, *13*, 1445. [[CrossRef](#)]
65. Kendall, M.G. *Rank Correlation Methods*, 4th ed.; Griffin, C., Ed.; Oxford University Press: New York, NY, USA, 1975; ISBN 0195208374.

Disclaimer/Publisher's Note: The statements, opinions and data contained in all publications are solely those of the individual author(s) and contributor(s) and not of MDPI and/or the editor(s). MDPI and/or the editor(s) disclaim responsibility for any injury to people or property resulting from any ideas, methods, instructions or products referred to in the content.